Tuning valley splitting and magnetic anisotropy of multiferroic CuMP$_2X_6$ (M = Cr, V; X = S, Se) monolayer

Dehe Zhang,[1] Aolin Li,[2] Xincheng Chen,[1] Wenzhe Zhou,[2,*] and Fangping Ouyang[1,2,3,†]

[1]*School of Physics and Electronics, Hunan Key Laboratory for Super-Microstructure and Ultrafast Process, and Hunan Key Laboratory of Nanophotonics and Devices, Central South University, Changsha 410083, People's Republic of China*

[2]*State Key Laboratory of Powder Metallurgy, and Powder Metallurgy Research Institute, Central South University, Changsha 410083, People's Republic of China*

[3]*School of Physics and Technology, Xinjiang University, Urumqi 830046, People's Republic of China*

(Received 24 November 2021; revised 20 January 2022; accepted 25 January 2022; published 8 February 2022)

Monolayer CuMP$_2X_6$ (M = Cr, V; X = S, Se) has been attracting increasing attention due to the ferromagnetism derived from the indirect exchange interaction between Cr (V) atoms and the ferroelectricity originating from the spontaneous displacement of Cu atoms. Using first-principles calculations, we predicted the intrinsic valley splittings and anomalous valley Hall effect in CuMP$_2X_6$ monolayers. In addition, the valley splittings and Berry curvature are independent of the orientation of out of plane (OOP) ferroelectric polarization, which makes it a promising storage device with dual degrees of freedom in ferroelectric polarization and ferrovalleys. Due to the variations in the energy of the spin-dependent valence-band maximum (VBM) and orbital compositions of the valleys, the magnitude of valley splitting at VBM can be effectively tuned by the biaxial strain and external electric field. Large OOP magnetic anisotropy can be obtained by changing the energy and occupation (unoccupation) states of d orbital compositions through strain and charge doping, respectively, and the magnetic anisotropy of CuMP$_2X_6$ increases with increasing tensile biaxial strain from -5% to 5%. Our research results are expected to tune the valley splittings and magnetic anisotropy of CuMP$_2X_6$ and to help understand the physical mechanism.

DOI: 10.1103/PhysRevB.105.085408

I. INTRODUCTION

In addition to charge and spin, valley is another degree of freedom for Bloch electrons in the periodic structure [1–3]. Valley polarization was first realized on Si (100) under zero magnetic field [4], and the valley-dependent Berry curvatures in two-dimensional (2D) materials contribute to the valley Hall effect (VHE) [1]. The degenerate energy of a polarized valley can be lifted by applying an external magnetic field [5–9] or intrinsic exchange interaction [10–12], which is the so-called ferrovalley. In addition, valley-polarized materials can cause large valley splittings through magnetic proximity effects such as magnetic atom doping [13] or ferromagnetic substrate [14–16]. Changing the magnitude of the external magnetic field is the most direct way to tune valley splitting, but the valley splitting of $MoSe_2$ had a weak response (0.22 meV/T) to external magnetic field in a previous study [5]. How to tune valley splitting and explain the physical mechanism of it remain unclear.

Multiferroics exhibit two or more primary ferroic orders among (anti)ferromagnetism, (anti)ferroelectricity, and ferroelasticity, and are drawing increasing interest because of the coupling of different ferroic orderings and application in novel electronic devices [17,18]. As the thickness of the material decreases, the depolarization field increases rapidly, so research studies mainly have focused on three-dimensional (3D) multiferroic perovskites, such as $TbMnO_3$ [19] and $BiFeO_3$ [20] in previous decades. With the rapid development of two-dimensional (2D) materials in recent years [21,22], researchers have discovered some novel 2D multiferroics, which avoid dangling bonds and quantum tunneling currents to break the size limit of traditional 3D semiconductor devices. Several theoretical works have predicted 2D multiferroic materials through atom adsorption or charge doping [23–25]. Furthermore, by van der Waals engineering and the stacking effect, multiple ferroic properties can coexist in bilayer and multilayer materials [26,27]. However, only a few intrinsic monolayer multiferroics have been reported [28–30]. Remarkably, monolayer multiferroic CuMP$_2X_6$ was recently discovered to be ferromagnetic, ferroelectric, and ferrovalley [31–33], but the intrinsic magnetic anisotropy energy (MAE) (less than 0.2 meV/unit cell) and valley splittings (less than 50 meV) are minor due to the orbital magnetic moment being annihilated by crystal field and weak spin-orbit coupling (SOC) of light atoms.

Using first-principles theory, we perform systematic research on the electronic structure and magnetic properties of monolayer CuMP$_2X_6$ (M = Cr, V; X = S, Se). We demonstrate that the valleys with opposite momentum at the VBM possess roughly opposite Berry curvatures. We provide a way to tune valley splittings through changing the energy of the spin-dependent band and orbital compositions of the valleys,

*csuzwz18@csu.edu.cn
†ouyangfp06@tsinghua.org.cn

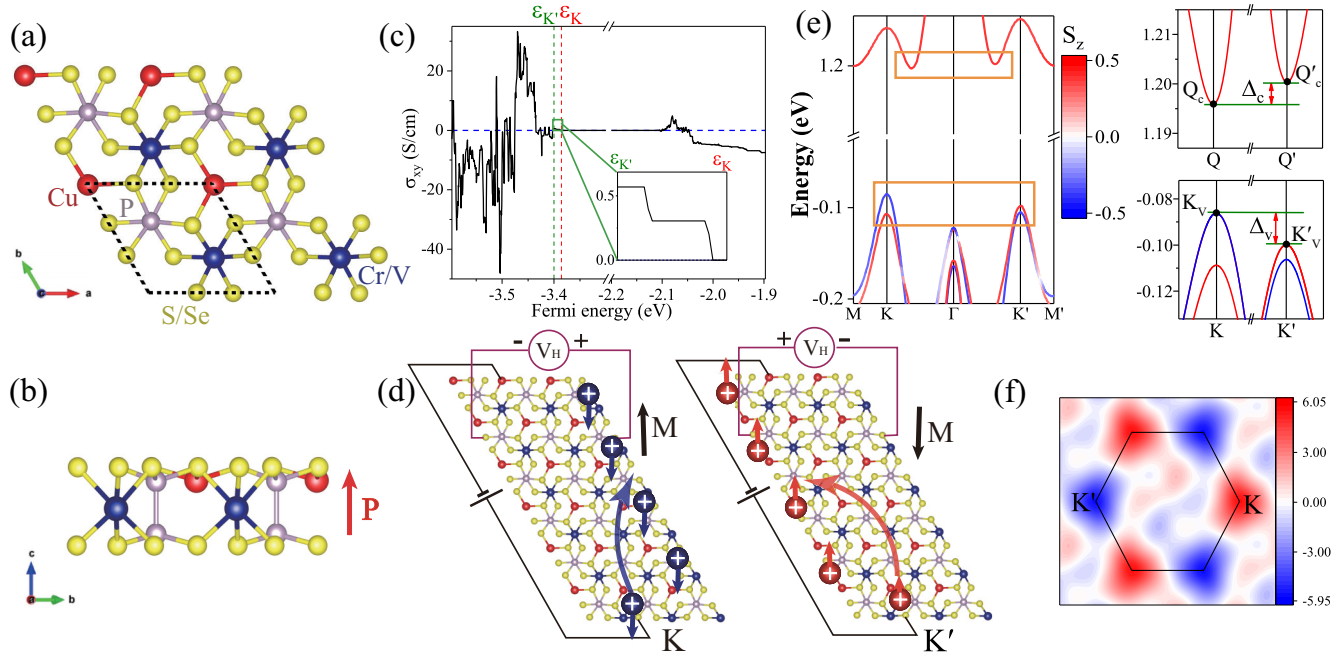

FIG. 1. (a) Top view and (b) side view of the crystal structure of monolayer CuMP$_2X_6$ (M = Cr, V; X = S, Se). The rhombus with dashed lines in (a) indicates the unit cell. (c) Fermi level dependent anomalous Hall conductivity σ_{xy} of monolayer CuCrP$_2$S$_6$. The two vertical dashed lines denote the energy of two valley extrema. The inset is the conductivity between the two dashed lines. (d) The schematic diagram of the AVHE of monolayer CuCrP$_2$S$_6$. The black arrow denotes the orientation of magnetic moments. (e) The band structures with SOC (left) and the magnified views (right) in the orange box of the bottom conduction bands (up) and top valence bands (down). Δ_c and Δ_v denote the valley splittings at the CBM and VBM, respectively. (f) The Berry curvatures in the 2D Brillouin zone of monolayer CuCrP$_2$S$_6$.

which also contributes to understanding the physical mechanism of the valley splitting. In addition, through analysis of the orbital interaction between the unoccupied states and the occupied states, the change in the MAE is perfectly explained, and we obtain large OOP magnetic anisotropy, which is beneficial for stabilizing the orientation of magnetic moments against thermal fluctuation.

II. COMPUTATIONAL DETAILS

All structural optimization and electronic structure calculations have been performed using the Vienna *ab initio* simulation package (VASP) [34] based on density functional theory (DFT). The Perdew-Burke-Ernzerhof (PBE) exchange-correlation functional was employed for the generalized gradient approximation (GGA) [35]. The electron-ion interaction was treated by the projector augmented wave (PAW) [36] method and the plane-wave basis was set to a cutoff energy of 500 eV. A vacuum slab of 20 Å was applied along the z direction making it possible to ignore the interaction between repeated slabs. Dipole correction is applied to avoid the interaction between electrical polarization in the periodic structure [37]. Referring to previous work [38], the PBE-D3 empirical correction method [39] was considered for taking the internal van der Waals interaction into account. The structural optimization was fully relaxed until the force on each atom was less than 0.01 eV/Å and the energy difference between the two adjacent steps was less than 10^{-6} eV, and an $8 \times 8 \times 1$ Γ-centered k-point grid was adopted for the k-point sampling. To treat localized d orbitals, we applied Hubbard U corrections with $U_{\text{eff}} = 3.0$ eV for Cr (V) atoms, which has been tested in previous research [31,32,40]. Berry curvature and anomalous Hall conductivity are calculated by using the maximally localized Wannier function method as implemented in the WANNIER90 package [41].

III. RESULTS AND DISCUSSION

Layered CuMP$_2X_6$ bulk is self-assembled through weak interlayer van der Waals interaction and it has been synthesized in previous experiments [42]. Monolayer CuMP$_2X_6$ consists of two parallel-arranged hexagonal S (Se) sheets; the Cu, Cr (V), and P-P bonds are located inside the octahedron composed of S (Se) atoms, as shown in Fig. 1. Cu atoms deviate perpendicularly from the center of the octahedron, resulting in an OOP electrical polarization. The orientation of Cu atom displacement in the OOP can be controlled by an external electric field to achieve the inversion of the OOP polarization, which is the origin of the ferroelectricity. In addition, since there are unoccupied 3d orbitals of the Cr (V) atoms, monolayer CuMP$_2X_6$ exhibits internal ferromagnetism with 3 (2) μ_B magnetic moments per unit cell. It is more intriguing that under the intrinsic exchange interaction and SOC, CuMP$_2X_6$ produces a spontaneous ferrovalley effect.

Monolayer CuCrP$_2$S$_6$ is an indirect semiconductor with VBM at the $K_v(K'_v)$ point and conduction-band minimum (CBM) at the $Q_c(Q'_c)$ point as shown in Fig. 1(e). The energy of $K_v(Q_c)$ and $K'_v(Q'_c)$ with opposite momentum is degenerate without SOC, but spin splitting occurs in the top valence band due to the existence of two bands of similar energy with

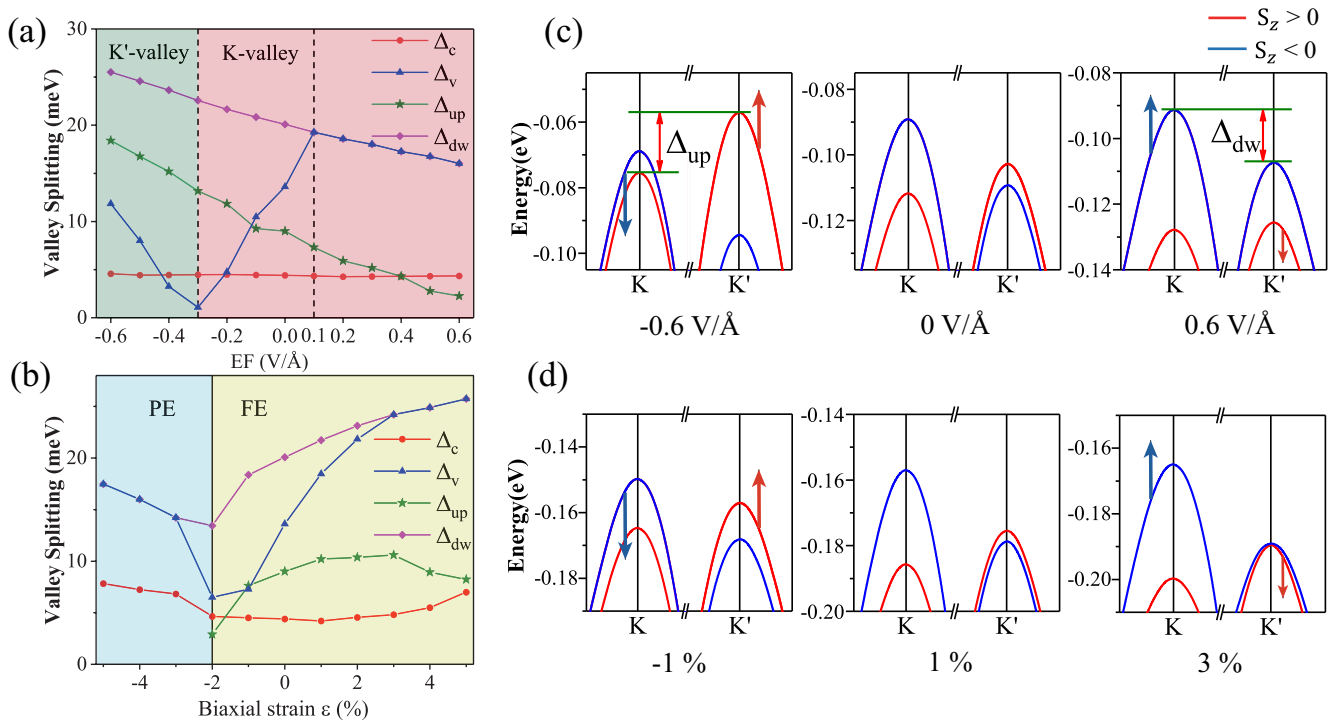

FIG. 2. The variations of valley splitting of monolayer $CuCrP_2S_6$ as a function of an external electric field (a) and IP biaxial strain (b). The light red and light green areas in (a) denote the VBM at the K- and K'-valley, respectively. The light yellow and light blue areas in (b) denote the ferroelectric (FE) phase and paraelectric (PE) phase, respectively. The top valence-band structures near the K and K' points at an external electric field (c) and biaxial strain (d). Δ_{up} and Δ_{dw} in (c) denote the valley splittings at the spin-up VBM and spin-down VBM of monolayer $CuCrP_2S_6$, respectively. The red (blue) arrow denotes the movement of spin-up (-down) VBM compared with 0 V/Å electric field (1% biaxial strain).

opposite spin channels near the top valence band (see Supplemental Material [43]). When SOC is considered, the energy of $K_v(Q_c)$ and $K'_v(Q'_c)$ will not degenerate, and the valley splitting is 13.6 (4.4) meV. Therefore the valley splitting depends on the strength of the SOC. The Hamiltonian of the SOC can be written as

$$H_{\text{soc}} = \lambda(L_+S_+ + L_-S_- + L_zS_z), \tag{1}$$

where λ represents the SOC coefficient, and L, S are the orbital and spin angular momentum, respectively. Since the spin is along the z axis, the magnitude of the valley splitting depends on the magnitude of L_z. The $Q_c(Q'_c)$ point is mainly composed of the p orbital and the OOP d_{xz} orbital. In contrast, the $K_v(K'_v)$ point is contributed by more in-plane (IP) orbitals d_{xy} and $d_{x^2-y^2}$ (see Supplemental Material [43]). Since L_z of the IP d_{xy} and $d_{x^2-y^2}$ orbitals is larger than that of the OOP d_{xz} orbitals, the valley splitting at VBM (Δ_v) is larger than at CBM (Δ_c), as shown in Fig. 1(e). Berry curvature can be considered as a pseudomagnetic field in momentum space. Figure 1(f) shows the Berry curvature in momentum space; the K and K' points have Berry curvatures with opposite sign but different magnitude, about 5.6 and -5.5 (Å^2), respectively. The Fermi level dependent anomalous Hall conductance can be obtained by integrating the Berry curvature over the Brillouin zone. The Hall conductivity σ_{xy} in Fig. 1(c) is different at the two valley extrema ε_k and $\varepsilon_{k'}$. Through hole doping, fully polarized spin and valley carriers can be generated. Therefore the intrinsic ferrovalley nature will produce an AVHE, and the schematic diagram is shown in Fig. 1(d). When the orientation of magnetization is upward, under the action of an IP electric field, the spin-down holes of a K valley in the light p type doped monolayer $CuCrP_2S_6$ shift to the right edge under the effective magnetic field generated by the Berry curvature, which generates a positive lateral Hall voltage. When the orientation of magnetization is downward, the valley splittings will also be reversed and the spin-up holes of the K'-valley shift to the left edge, generating a negative lateral Hall voltage, which can be used to store and read information. The orientation of OOP ferroelectric polarization can be reversed by the Cu atoms shifting to the S atoms on the other side. However, the valley splitting and Berry curvature remain unchanged with the reversal of the OOP ferroelectric polarization (see Supplemental Material [43]). Therefore, the independence of ferroelectricity and AVHE makes Cu Cr $P_2S(Se)_6$ a promising storage device with dual degrees of freedom.

Generally, the external electric field has a very great effect on ferroelectric materials. We researched the response of valley splittings to the OOP electric field. It is found that the valley splitting Δ_c at the CBM is not sensitive to the OOP electric field. Remarkably, with the increase of the positive electric field, the energy of the spin-down VBM gradually increases compared to the spin-up VBM as seen in Fig. 2(c). Therefore the valley splitting Δ_v at the VBM gradually approaches the valley splitting Δ_{dw} at the spin-down VBM, and they are completely equal when a positive electric field of 0.1

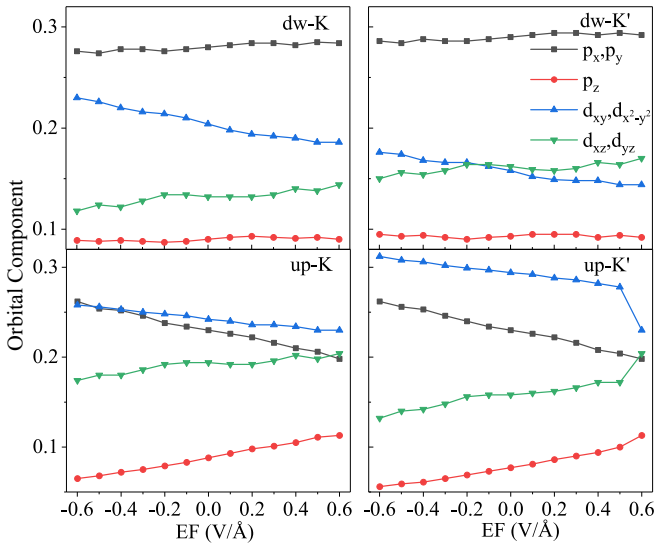

FIG. 3. The variations of orbital components at the K and K' points of the spin-down VBM and spin-up VBM of monolayer $CuCrP_2S_6$ as a function of an external electric field.

V/Å is applied. When a negative electric field of 0.4 V/Å is applied, the energy of the spin-up VBM (K' valley) is higher than the spin-down VBM (K valley), the VBM moves from K to K', and the spin direction of VBM transforms from down to up. Therefore we can reverse the spin direction and valley splitting at VBM by applying an electric field instead of a magnetic field, which means the coupling of electricity and ferrovalley. In addition, when a negative electric field of more than 0.4 V/Å is applied, the deflection direction and the spin direction of the hole carriers will be reversed in the AVHE. More intriguing is that the valley split Δ_{dw} and Δ_{up} decrease monotonously with the increase of the positive electric field. As shown in Fig. 3, for the spin-down VBM, the contribution of the IP orbitals d_{xy} and $d_{x^2-y^2}$ decreases and the contribution of the OOP orbitals d_{xz} and d_{yz} increases with the increase of the positive electric field, which makes the L_z at the K and K' valley of the spin-down VBM decrease continuously, so the spin split Δ_{dw} caused by SOC decreases. At the K (K') valley of the spin-up VBM, the change trend of the d orbital components are the same as the K (K') valley of the spin-down VBM, so Δ_{up} decreases continuously with the increase of the positive electric field. In particular, the contribution of the p orbital components at the K (K') valley of the spin-up VBM has also changed significantly. The contribution of the IP p_x and p_y orbitals decreases with the increase of the positive electric field, and the contribution of the OOP p_z orbitals increases with the increase of the positive electric field. The contribution of p orbitals to H_{soc} and the contribution of the interaction of p orbitals and d orbitals to H_{soc} may be the reason why the valley splitting Δ_{up} changes with an electric field greater than Δ_{dw}.

IP biaxial strain is also applied to research the response of valley splittings. As shown in Fig. 2(a), when a compressive strain of 3% is applied, the valley splittings at the CBM and VBM of $CuCrP_2S_6$ undergo abrupt changes due to the transition from the ferroelectric phase to the paraelectric phase. In the same way as the applied electric field, the valley splitting at the CBM of $CuCrP_2S_6$ is not sensitive to strain. The valley splitting at the VBM of the ferroelectric phase increases with

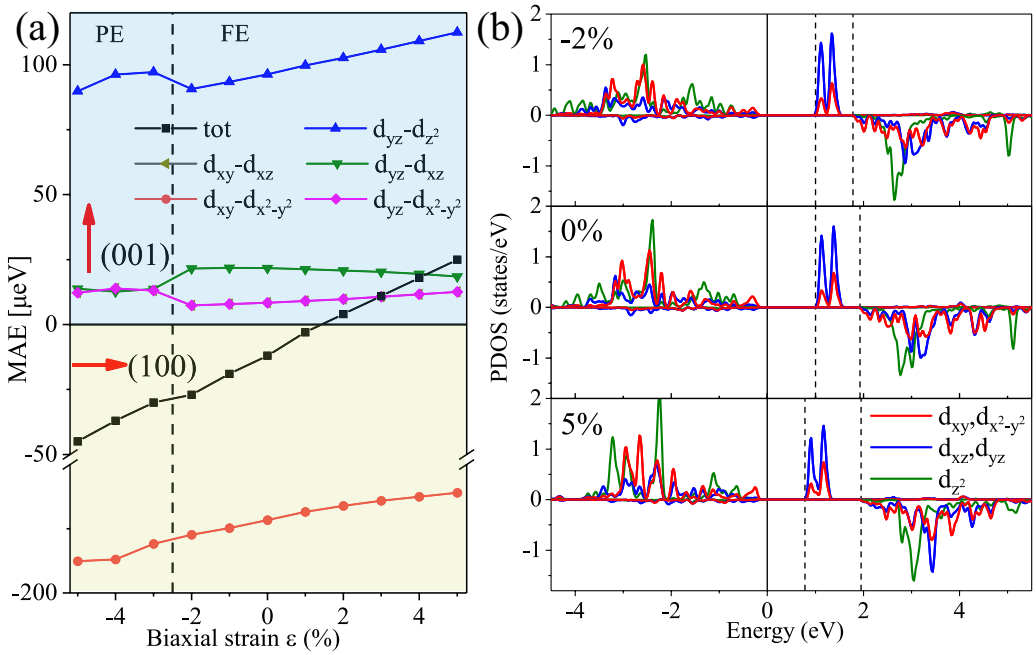

FIG. 4. (a) The variations of total MAE and projected orbital coupling matrix elements of monolayer $CuCrP_2S_6$ as a function of an IP biaxial strain. The light yellow and light blue areas denote IP magnetic anisotropy and OOP magnetic anisotropy, respectively; the red arrows denote the most stable orientation of magnetic moments, and the ones in Fig. 5(a) are the same. (b) The d orbital PDOS near the Fermi level of Cr atoms of monolayer $CuCrP_2S_6$ under a -2%, 0% and 5% biaxial strain. The black solid line denotes Fermi level, and the two vertical black dashed lines denote the bottom of spin-up and spin-down unoccupied states.

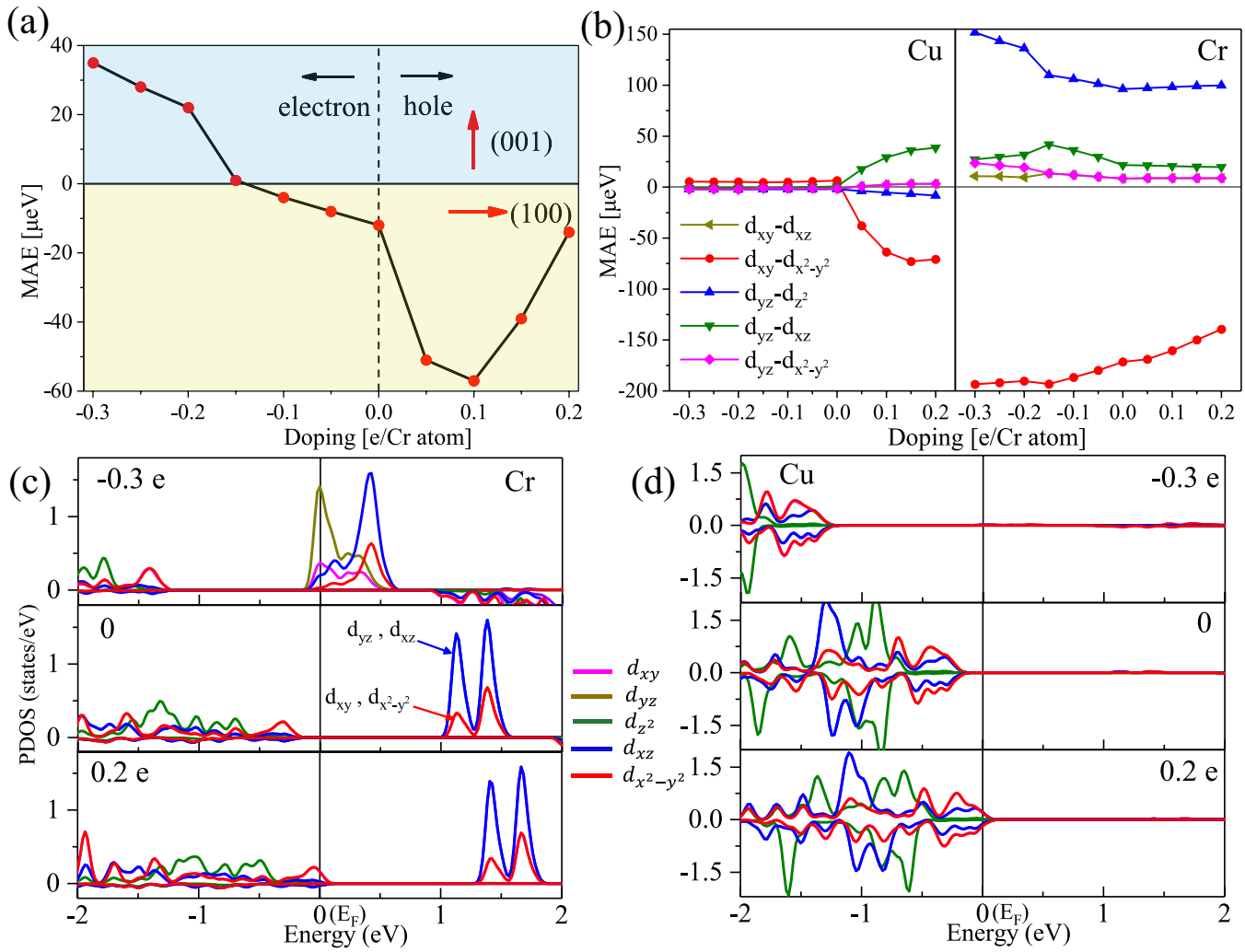

FIG. 5. The variations of total MAE (a) and projected orbital coupling matrix elements of Cu and Cr atoms (b) of monolayer $CuCrP_2S_6$ as a function of charge doping. The black arrows in (a) denote the hole or electron doping. The d orbital PDOS near the Fermi level of Cr atoms (c) and Cu atoms (d) of monolayer $CuCrP_2S_6$ under a −0.3, 0, and 0.2 (e/Cr atom) charge doping.

the increase of the tensile strain. This is because the energy of the spin-down VBM gradually increases compared to the spin-up VBM during the tensile strain as seen in Fig. 2(d). Therefore the valley splitting Δ_v gradually approaches Δ_{dw}, and is completely equal when a 3% tensile strain is applied.

In the practical application of 2D magnetic materials, we usually prefer a large uniaxial magnetic anisotropy to stabilize the orientation of the magnetic moment and form a long-range magnetic order under a finite temperature. According to the second-order perturbation theory [44], the MAE consists of two items, where the contributions of the same spin channel with upward orientation (uu) and downward orientation (dd) can be expressed as

$$\mathrm{MAE} = E_x - E_z = \xi^2 \sum_{o,u} \frac{|\langle o|L_z|u\rangle|^2 - |\langle o|L_x|u\rangle|^2}{E_u - E_o}, \quad (2)$$

where o (u) stand for the occupied (unoccupied) states, and the energy of occupied (unoccupied) states is represented by E_o (E_u); L_z and L_x are the angular momentum operators. Likewise, the contributions of the coupling between opposite spin channel (ud) can be expressed as

$$\mathrm{MAE} = E_x - E_z = \xi^2 \sum_{o,u} \frac{|\langle o|L_x|u\rangle|^2 - |\langle o|L_z|u\rangle|^2}{E_u - E_o}. \quad (3)$$

For the d orbitals, the nonzero contribution comes from $\langle d_{xy}|L_z|d_{x^2-y^2}\rangle$, $\langle d_{yz}|L_z|d_{xz}\rangle$, $\langle d_{yz}|L_x|d_{z^2}\rangle$, $\langle d_{xy}|L_x|d_{xz}\rangle$, and $\langle d_{yz}|L_x|d_{x^2-y^2}\rangle$. As shown in Fig. 5(d), the filled d orbital electrons of Cu atoms do not contribute to the unoccupied states, so the MAE of monolayer $CuCrP_2S_6$ under biaxial strain is derived from the coupling between the d orbitals of Cr atoms. As the tensile strain increases, the increase of the MAE of the ferroelectric phase is mainly due to the increasing positive magnetic anisotropy contributed by $\langle d_{xy}|L_z|d_{x^2-y^2}\rangle$ and $\langle d_{yz}|L_x|d_{z^2}\rangle$, as seen in the projected orbital coupling matrix elements in Fig. 4(a). In the projected density of states (PDOS) in Fig. 4(b), the d orbital electron of the occupied states of Cr atoms near the Fermi level is the same spin-up; the spin-up occupied states are coupled with spin-up unoccupied states (uu term) closer to the Fermi level and spin-down unoccupied states (ud term) farther from the Fermi

level. Since the number of the spin-down electrons is far more than spin-up electrons in the unoccupied states of Cr atoms, the ud term dominates the MAE. As the tensile strain increases, the energy of spin-up unoccupied states decreases, so the $\langle d_{xy}|L_z|d_{x^2-y^2}\rangle$ of the positive MAE in the uu term increases, and the energy of spin-down unoccupied states increases, so the $\langle d_{xy}|L_z|d_{x^2-y^2}\rangle$ of the negative MAE in the ud term decreases; therefore the total $\langle d_{xy}|L_z|d_{x^2-y^2}\rangle$ increases. In addition, as the tensile strain increases, the energy of the occupied d_{z^2} increases, so that the contribution of the dominant ud term of $\langle d_{yz}|L_x|d_{z^2}\rangle$ to MAE is positive and increases. The MAE of other CuMP$_2X_6$ also increases with increasing tensile strain (see Supplemental Material [43]).

Charge doping can not only get the AVHE, but also adjust the MAE of monolayer CuMP$_2X_6$ to a large extent. When electrons (holes) are doped, the change in the MAE is mainly due to the transition between the occupied and unoccupied states of the orbitals. As shown in Figs. 5(c) and 5(d), when electrons are doped, the original energy degenerate $d_{x^2-y^2}$ and d_{xy} (d_{yz} and d_{xz}) orbitals are split, the spin-up d_{yz} orbital transforms from unoccupied state to occupied state, and it couples with the spin-down d_{z^2} orbital (ud-$\langle d_{yz}|L_x|d_{z^2}\rangle$) to contribute a positive MAE, which increases monotonously, so the orientation of the easy axis of magnetization transforms from IP to OOP. When holes are doped, the difference from the previous discussion is that the $d_{x^2-y^2}$, d_{xy}, d_{yz}, and d_{xz} orbitals of the Cu atom transform from occupied state to unoccupied state, and couple with occupied states to contribute the MAE, in which $\langle d_{xy}|L_z|d_{x^2-y^2}\rangle$ contributes a larger negative MAE, and $\langle d_{yz}|L_z|d_{xz}\rangle$ contributes a smaller positive MAE. In addition, the $d_{x^2-y^2}$ and d_{xy} orbitals of the Cr atom transform from occupied state to unoccupied state, and couple with the spin-up $d_{x^2-y^2}$ and d_{xy} orbitals (uu-$\langle d_{xy}|L_z|d_{x^2-y^2}\rangle$) to contribute a positive MAE. The results we obtained from the previous analysis of the PDOS are in good agreement with the variations of orbital coupling matrix elements in Fig. 5(b). Therefore, the competition between the positive MAE contributed by Cr atoms and the negative MAE contributed by Cu atoms makes the MAE of $CuCrP_2S_6$ first decrease and then increase when holes are doped, and the MAE of other CuMP$_2X_6$ can be effectively adjusted by charge doping as shown in the Supplemental Material [43].

IV. CONCLUSIONS

In summary, based on first-principles calculations, we investigated the valley splittings and magnetic anisotropy of multiferroic CuMP$_2X_6$ monolayer. It is found that the valleys of $CuCrP_2X_6$ have Berry curvature with opposite signs and different magnitude, and the energy splitting of the valleys will cause an AVHE. When an external electric field or IP biaxial strain is applied, the valley splitting at the CBM (Δ_c) has no obvious change, but the valley splitting at the VBM (Δ_v) undergoes obvious change, which is mainly due to the relative movement between the spin-down VBM and the spin-up VBM. The variations of the IP and OOP orbital compositions at the valleys cause the valley splitting at the spin-down (-up) VBM to change. Magnetic anisotropy is also affected by IP biaxial strain. Due to the energy changes of the d orbital compositions of the Cr (V) atom, the MAE of CuMP$_2X_6$ increases with increasing tensile strain. When charge doping is performed, the occupation (unoccupation) states of the d orbital components near the Fermi level will be changed, so that a large OOP magnetic anisotropy of CuMP$_2X_6$ can be obtained in the case of electronic doping. Our work provides a way to manipulate the valley splittings and magnetic anisotropy of novel 2D multiferroics.

ACKNOWLEDGMENTS

This paper was financially supported by the National Natural Science Foundation of China (Grants No. 52073308 and No. 11804395), the Distinguished Young Scholar Foundation of Hunan Province (Grant No. 2015JJ1020), the Central South University Research Fund for Sheng-hua Scholars (Grant No. 502033019), and the Postgraduate Research Innovation Project of Central South University (Grant No. 1053320210136). This work was carried out in part using computing resources at the High Performance Computing Center of Central South University.

[1] D. Xiao, W. Yao, and Q. Niu, Phys. Rev. Lett. **99**, 236809 (2007).
[2] S. A. Wolf, D. D. Awschalom, R. A. Buhrman, J. M. Daughton, S. von Molnar, M. L. Roukes, A. Y. Chtchelkanova, and D. M. Treger, Science **294**, 1488 (2001).
[3] J. R. Schaibley, H. Yu, G. Clark, P. Rivera, J. S. Ross, K. L. Seyler, W. Yao, and X. Xu, Nat. Rev. Mater. **1**, 16055 (2016).
[4] K. Takashina, Y. Ono, A. Fujiwara, Y. Takahashi, and Y. Hirayama, Phys. Rev. Lett. **96**, 236801 (2006).
[5] D. MacNeill, C. Heikes, K. F. Mak, Z. Anderson, A. Kormányos, V. Zólyomi, J. Park, and D. C. Ralph, Phys. Rev. Lett. **114**, 037401 (2015).
[6] A. Srivastava, M. Sidler, A. V. Allain, D. S. Lembke, A. Kis, and A. Imamoğlu, Nat. Phys. **11**, 141 (2015).
[7] Y. P. Shkolnikov, E. P. De Poortere, E. Tutuc, and M. Shayegan, Phys. Rev. Lett. **89**, 226805 (2002).
[8] P. Recher, J. Nilsson, G. Burkard, and B. Trauzettel, Phys. Rev. B **79**, 085407 (2009).
[9] T. Smoleński, M. Goryca, M. Koperski, C. Faugeras, T. Kazimierczuk, A. Bogucki, K. Nogajewski, P. Kossacki, and M. Potemski, Phys. Rev. X **6**, 021024 (2016).
[10] Z. Song, X. Sun, J. Zheng, F. Pan, Y. Hou, M. H. Yung, J. Yang, and J. Lu, Nanoscale **10**, 13986 (2018).
[11] W. Y. Tong, S. J. Gong, X. Wan, and C. G. Duan, Nat. Commun. **7**, 13612 (2016).
[12] C. M. Zhang, Y. H. Nie, S. Sanvito, and A. J. Du, Nano Lett. **19**, 1366 (2019).
[13] Y. C. Cheng, Q. Y. Zhang, and U. Schwingenschlögl, Phys. Rev. B **89**, 155429 (2014).
[14] Q. Zhang, S. A. Yang, W. Mi, Y. Cheng, and U. Schwingenschlogl, Adv. Mater. **28**, 959 (2016).
[15] K. L. Seyler, D. Zhong, B. Huang, X. Linpeng, N. P. Wilson, T. Taniguchi, K. Watanabe, W. Yao, D. Xiao, M. A. McGuire, K. C. Fu, and X. Xu, Nano Lett. **18**, 3823 (2018).
[16] W. Zhou, Z. Yang, A. Li, M. Long, and F. Ouyang, Phys. Rev. B **101**, 045113 (2020).

[17] C. A. F. Vaz, J. Hoffman, C. H. Ahn, and R. Ramesh, Adv. Mater. **22**, 2900 (2010).
[18] W. Eerenstein, N. D. Mathur, and J. F. Scott, Nature (London) **442**, 759 (2006).
[19] T. Kimura, T. Goto, H. Shintani, K. Ishizaka, T. Arima, and Y. Tokura, Nature (London) **426**, 55 (2003).
[20] J. Wang, J. B. Neaton, H. Zheng, V. Nagarajan, S. B. Ogale, B. Liu, D. Viehland, V. Vaithyanathan, D. G. Schlom, U. V. Waghmare *et al.*, Science **299**, 1719 (2003).
[21] C. L. Tan, X. H. Cao, X. J. Wu, Q. Y. He, J. Yang, X. Zhang, J. Z. Chen, W. Zhao, S. K. Han, G. H. Nam, M. Sindoro, and H. Zhang, Chem. Rev. **117**, 6225 (2017).
[22] K. S. Novoselov, A. Mishchenko, A. Carvalho, and A. H. C. Neto, Science **353**, aac9439 (2016).
[23] C. Huang, Y. Du, H. Wu, H. Xiang, K. Deng, and E. Kan, Phys. Rev. Lett. **120**, 147601 (2018).
[24] Q. Yang, W. Xiong, L. Zhu, G. Gao, and M. Wu, J. Am. Chem. Soc. **139**, 11506 (2017).
[25] Z. Tu, M. Wu, and X. C. Zeng, J. Phys. Chem. Lett. **8**, 1973 (2017).
[26] X. Liu, A. P. Pyatakov, and W. Ren, Phys. Rev. Lett. **125**, 247601 (2020).
[27] C. Gong, E. M. Kim, Y. Wang, G. Lee, and X. Zhang, Nat. Commun. **10**, 2657 (2019).
[28] H. Wang and X. F. Qian, 2D Mater. **4**, 015042 (2017).
[29] J. J. Zhang, L. F. Lin, Y. Zhang, M. H. Wu, B. I. Yakobson, and S. Dong, J. Am. Chem. Soc. **140**, 9768 (2018).
[30] Y. J. Sun, T. Feng, X. L. Li, F. Wu, H. F. Lv, and X. J. Wu, J. Mater. Chem. C **9**, 9197 (2021).
[31] J. Qi, H. Wang, X. Chen, and X. Qian, Appl. Phys. Lett. **113**, 043102 (2018).
[32] Y. Lai, Z. Song, Y. Wan, M. Xue, C. Wang, Y. Ye, L. Dai, Z. Zhang, W. Yang, H. Du and J. Yang, Nanoscale **11**, 5163 (2019).
[33] M. A. Susner, R. Rao, A. T. Pelton, M. V. McLeod, and B. Maruyama, Phys. Rev. Mater. **4**, 104003 (2020).
[34] G. Kresse and J. Furthmüller, Phys. Rev. B **54**, 11169 (1996).
[35] J. P. Perdew, K. Burke, and M. Ernzerhof, Phys. Rev. Lett. **77**, 3865 (1996).
[36] G. Kresse and D. Joubert, Phys. Rev. B **59**, 1758 (1999).
[37] G. Makov and M. C. Payne, Phys. Rev. B **51**, 4014 (1995).
[38] S. A. Tawfik, J. R. Reimers, C. Stampfl, and M. J. Ford, J. Phys. Chem. C **122**, 22675 (2018).
[39] S. Grimme, J. Antony, S. Ehrlich, and H. Krieg, J. Chem. Phys. **132**, 154104 (2010).
[40] X. K. Ma, L. Sun, J. Liu, X. K. Feng, W. F. Li, J. F. Hu, and M. W. Zhao, Phys. Status Solidi RRL **14**, 2000008 (2020).
[41] A. A. Mostofi, J. R. Yates, G. Pizzi, Y. S. Lee, I. Souza, D. Vanderbilt, and N. Marzari, Comput. Phys. Commun. **185**, 2309 (2014).
[42] M. A. Susner, M. Chyasnavichyus, M. A. McGuire, P. Ganesh, and P. Maksymovych, Adv. Mater. **29**, 1602852 (2017).
[43] See Supplemental Material at http://link.aps.org/supplemental/10.1103/PhysRevB.105.085408 for more details on the projected band structure, Berry curvatures, and magnetic anisotropy energy of the $CuMP_2X_6$ (M = Cr, V; X = S, Se) monolayer.
[44] D.-s. Wang, R. Wu, and A. J. Freeman, Phys. Rev. B **47**, 14932 (1993).